Microstructure and Mechanical Characterization of Rapidly Solidified Cr-C Tool Steel: Annealing Effects

P. Delshad Khatibi[1], H. Henein[1], A.B. Phillion[2]
Corresponding Author: andre.phillion@ubc.ca

[1] Chemical and Materials Engineering Department, University of Alberta
Edmonton, Alberta, T6G 2V4, Canada
[2] Department of Materials Science and Engineering, McMaster University, Hamilton, Ontario, L8S 4L7, Canada

Abstract

The effect of isochronal annealing on D2 tool steel powder, rapidly solidified via both Impulse Atomization and Water Atomization, has been evaluated using high-resolution scanning electron microscopy and Vickers microhardness. The amount of supersaturation of the alloying elements inside the retained austenite phase as a function of eutectic undercooling was calculated. The fraction of austenite transformed to ferrite at different annealing temperatures (from 350°C to 810°C) was also determined, using Rietveld analysis. The results show that although the particles with larger eutectic undercooling have larger supersaturation of alloying elements within the retained austenite phase, they have a smaller fraction of austenite to ferrite transformation at the temperature in which transformation starts. The maximum hardness was achieved at an annealing temperature of 550°C, due to the formation of fine and well-distributed carbides.

Introduction

D2 tool steel is a well-known high-chromium and high-carbon ferrous alloy that can be found in many industrial applications. This material has a high volume fraction of carbides, which results in good wear and abrasion properties. The $(Fe,Cr)_7C_3$ carbide has a hardness in the 1300-1800 HV range [1]. For wear applications, a conventional tool steel casting process is used to make D2 tool steel components, due to the resulting and beneficial coarse carbide structure. For other applications, D2 tool steel is normally cast using Rapid Solidification (RS) techniques [2]. This ensures the formation of a refined microstructure [3].

Although D2 tool steel is of high commercial significance, there have been relatively few studies that characterize its microstructure during RS processing. Two studies reported results from

material rapidly solidified using splat quenching and melt spinning [4,5]. Two others used x-ray diffraction and transmission electron microscopy [6,7] to show that RS of D2 tool steel results in the formation of a supersaturated metastable retained austenite phase, and that subsequent annealing results in the formation of rod-like carbide precipitates in a ferrite matrix.

During rapid solidification of tool steels, alloying elements do not have time to diffuse out of the austenite structure but remain supersaturated within it. These elements then precipitate out during subsequent annealing in the form of M_7C_3 carbides. The supersaturation of M_7C_3 carbides ($S_{M_7C_3}$) at a given annealing temperature is defined as [8]:

$$S_{M_7C_3} = \ln\left[\frac{X_M^7 \cdot X_C^3}{K_{M_7C_3}}\right]$$

Eq. 1

where X_M and X_C are the supersaturated concentrations of M (Cr, V, etc.) and C in mole fraction, and $K_{M_7C_3} = X_{eM}^7 \cdot X_{eC}^3$ is the equilibrium solubility product given by the equilibrium concentrations of M and C (denoted as X_{eM} and X_{eC}). Temperature-dependent equilibrium solubility products can be determined using a Calphad-type thermodynamics software package. The value of $K_{M_7C_3}$ in D2 tool steel, calculated using Thermo-calc [9], is:

$$\log K_{M_7C_3} = 19.1 - \frac{18639}{T}$$

Eq. 2

The research presented in this study forms the second of two recent studies in our research group examining the microstructural development of D2 tool steel produced via two rapid solidification methods: Impulse Atomization (IA) and Water Atomization (WA). The first study [10] evaluated the effects of the atomization process conditions on the rapidly solidified microstructure in the as-solidified state. From this study, it was shown that higher cooling rates result in a lower percentage of eutectic fraction. Consequently, the retained austenite would be supersaturated in carbide-forming elements. A summary of the experimental data from [10] linking eutectic fraction, cooling rate, and undercooling is given in Table 1. In the present study, the effect of annealing temperature on the microstructure of D2 tool steel is explored. Together, the two

studies provide a comprehensive analysis of microstructural development during rapid solidification processing of D2 tool steel.

Experimental

D2 tool steel is a high-carbon, high-chromium ferrous alloy with 1.55% C, 11.8% Cr, 0.40% Mn, 0.80% Mo, and 0.80% V (all in wt.%). The corresponding pseudobinary phase diagram has liquidus and eutectic temperatures of 1394°C and 1270°C, respectively [7], and is given in the first study [10]. In order to investigate the effect of annealing on the microstructure of RS D2 tool steel, particles produced using IA [11] and WA [12,13] were given an isochronal anneal for 2 hours at temperatures of 350˚C, 450˚C, 550˚C, 650˚C, 750˚C, and 810˚C in a protective nitrogen atmosphere. 810˚C was chosen as the highest annealing temperature to avoid the initiation of the ferrite-to-austenite phase transformation occurring at higher temperatures, as identified by Thermo-Calc. The heating and cooling rate prior and post anneal was ~0.33˚C/min. Although the cooling rate is relatively low for studying phase transformations, the isochronal anneal was carried out in a differential scanning calorimeter (owing to the size of the powder particles), and the captured cooling curves did not show any peaks related to other reactions during the cooling cycle. Thus, it can be inferred that additional reactions did not take place during cooling.

The powder from IA was generated using an apparatus available at the University of Alberta [11]. First, a bulk alloy was melted and held in an alumina crucible for about 30 minutes at 1600 ℃. Then, the liquid was pushed through orifices at the bottom of the crucible to create droplets via atomization. The falling liquid droplets were then cooled in both helium and nitrogen atmospheres having a maximum oxygen content of 8 ppm, and thus solidified before reaching the bottom of the atomization chamber. The production parameters and resulting powder sizes are shown in Table 2. The powder from WA was provided by the Hoeganaes Corporation (Cinnaminson, New Jersey, USA). The atomized particles were then annealed in a Setaram Labsys Evo Differential Scanning Calorimeter.

IA particles in the size ranges of 300-355 µm and 600-710 µm, solidified in both He and N_2, and WA particles in the size ranges of 90-110 µm and 300-355 µm were subsequently prepared for scanning electron microscopy (SEM), x-ray diffraction (XRD) and neutron diffraction (ND). IA in He provides significantly higher cooling rates during RS as compared to N_2 due to the higher thermal conductivity. Samples of the chosen particle sizes were mounted in epoxy, polished, and

carbon coated. First, SEM images of the microstructure were acquired using a JEOL 6301F, a Hitachi S-2700, and a Zeiss EVO LS15. Different instruments were used due to machine scheduling and availability. The diameter of the precipitated carbides was measured from the SEM images using the ImageJ software [14], while compositional variations were measured via EDX analysis on the Zeiss SEM that was equipped with a Bruker silicon drift detector. As carbide particles are irregular in shape, the term diameter refers to an average diameter based on several random measurements made of diagonal distances along the particle's cross-section. Second, XRD was performed using Co-Kα radiation in a Rigaku Denki Rotaflex RU-200B X-ray system for phase identification. High Energy XRD (HEXRD) was also performed, at Argonne National Laboratory. Third, ND was carried out using a neutron beam of 1.33A° wavelength at Atomic Energy of Canada Limited (AECL) in Chalk River, ON. Lattice parameters were extracted using GSAS software. Finally, Vickers microhardness measurements were performed on the as-atomized and annealed particles using a Buehler Tukon 1102 Vickers hardness tester. Thirty data points were collected for each measurement using a load of 100 gf and a dwell time of 10 s.

Results and Discussion

Qualitative Description of the Microstructure

The XRD results, performed on particles between 600-710 µm in size produced via IA in N_2, are given in Figure 1. The spectra for both the initial as-atomized particles and the particles that were subsequently annealed for 2 hours at temperatures between 350˚C to 810˚C are shown. As can be seen in the as-atomized spectrum, the as-atomized powders consist of the austenite phase. Thus, the rapid solidification of D2 tool steel resulted in supersaturated metastable retained austenite and the ferrite phase, in primary form, was completely suppressed. Further, the austenite in the rapidly solidified D2 tool steel (as-atomized) particles was so stable that none of it transformed to martensite even after being quenched in liquid nitrogen. Likely, the high supersaturation of austenite caused a significant decrease in the martensite start temperature. Bhargava et al. [5] showed that the lattice parameter of RS-produced austenite in D2 tool steel is about 1.5% larger than that for γ-Fe, indicating the substantial supersaturation of carbon and chromium in the austenite. Note that although the material in the as-atomized state contains a small amount of eutectic carbides, they do not appear in the XRD spectrum as their weight fraction was below the detection limit of the instrument. Further analysis of Figure 1 indicates that while

annealing at 350°C and 450°C did not change the type phases present within the particles, annealing at 550°C resulted in partial transformation of the retained austenite to ferrite and M_7C_3 carbides. This is shown within Figure 1 via the presence of both ferrite and low intensity peaks (tentatively indexed to M_7C_3) within the XRD spectrum at 550˚C. At higher annealing temperatures (i.e. 650°C, 750°C and 810°C), the retained austenite has fully decomposed since only ferrite and the M_7C_3 peaks are present in the XRD data. Thus, the transformation from metastable retained austenite to ferrite occurs at a minimum annealing temperature of approximately 550˚C and is accompanied by M_7C_3 carbide precipitation. As discussed in research by Zumsande et al. [27], annealing of Fe-Cr alloys in nitrogen at temperatures of 750˚C or more may lead to significant nitrogen update, resulting in the formation of nitride particles. However, no evidence of this mechanism were found in the atomized particles. Specifically, no nitrides were detected in any of the particles during analysis of the HEXRD data.

Figure 2 shows SEM images of annealed 600-710 μm particles produced under the same conditions as for Figure 1. Only the micrographs from 550˚C, 650˚C, 750˚C and 810˚C are given since only these annealing temperatures resulted in carbide precipitation. The original as-solidified microstructure is also shown in Figure 2.e. Each image is at a different magnification to highlight salient features. In Figure 2.a (T_{anneal} = 550˚C), both the primary grains that formed during RS and the decomposed austenite micro-constituents can be seen. This observation matches the XRD result shown in Figure 1 for 550˚C. Region (I) is the retained austenite phase, while Region II (the area with the white colour inside) contains the transformed ferrite and the chromium carbides. In Figure 2.b (T_{anneal} = 650˚C), a fine two-phase microstructure can be observed. This high-resolution micrograph indicates that almost all of the retained austenite (Region (I) in Figure 2.a) has transformed to ferrite and carbide when an annealing temperature of 650˚C is applied, and that the precipitates are very fine and rod-shaped with a diameter of about 50 nm. Figure 2.c and Figure 2.d show images after annealing at 750˚C and 810˚C. As expected, by increasing the annealing temperature, the carbides coarsen and become more rounded as compared to the distribution seen in Figure 2.b.

Quantitative Analysis

5

A comprehensive quantitative analysis was performed to assess the degree of supersaturation of the atomized D2 tool steel particles, followed by the degree of transformation during the isochronal annealing process, and finally carbide size distribution.

Degree of Supersaturation during Particle Annealing

Figures 3 and Figure 4 show the variation in supersaturation for different annealing temperatures (550˚C, 650˚C and 750˚C) as a function of eutectic undercooling and applied cooling rate during RS for various IA and WA particles. The relationship between eutectic fractions, eutectic undercooling, and cooling rate is given in Table 1. From these tables, the X_M and X_C values used in Eq. 1 were calculated by determining the amount of M and C remaining in the austenite after precipitation of the M_7C_3 carbide as part of the eutectic reaction during RS. For this calculation, the equilibrium fraction of the carbide phase within the eutectic was estimated using Thermo-Calc to be 62 wt.% assuming that stoichiometry is maintained. Further, it was assumed that the eutectic phase fraction at room temperature are the same as at the eutectic temperature.

As can be seen in Figures 3 and 4, the degree of supersaturation within the austenite phase is quite high. Eutectic undercooling and applied cooling rate during RS both significantly modify the results; larger values increase the degree of supersaturation within the retained austenite. Further, the level of supersaturation in the particles is higher at lower annealing temperatures. This is because the corresponding equilibrium solubility limit is smaller, and should lead to a finer precipitates assuming that the nucleation barrier to precipitation is overcome.

Degree of Transformation during Particle Annealing

In order to quantify the degree of transformation during the isochronal annealing, Rietveld analysis was carried out on the XRD data from particles that were 600-710 µm in size, produced via IA in N_2, and then annealed at temperatures between 350˚C and 810˚C. The profile refinement was performed using the software GSAS [15]. The process was first to determine the lattice parameter of the matrix phases (retained austenite, ferrite) as a function of annealing temperature and then to calculate the percentage of phase transformation that had occurred. Since the XRD peaks for the carbide phase were so weak, they were ignored in the analysis. The resulting lattice parameters and percent transformation as a function of annealing temperature are shown in Figure 5. As can be seen, the lattice parameter of the matrix phase and the percent transformation remain almost constant at 0.3623 nm and zero respectively at annealing temperatures up to 550℃. Then,

there is a sharp drop in lattice parameter from 0.3610 nm to 0.2871 nm as the retained austenite transforms to ferrite, and a steep rise in the value of percent transformation from zero to approximately 90%. Due to this phase transformation, it can be roughly estimated that carbide precipitation starts around 550°C, although additional experiments would be needed to determine the exact value between 450°C and 550°C. At 650°C and above, the lattice parameter remains approximately constant at 0.2871 nm since the entire matrix has 100% transformed to ferrite. While Li et al. [16] have reported that laser melted high chromium steel transforms from austenite to martensite during air cooling after annealing, no evidence of martensite was seen in the atomized particles studied in this work. The cooling rate after the isochronal anneal was about 0.33°C/min, which does not appear to be fast enough to form martensite from the retained austenite. In contrast, it seems that the cooling rate of the depleted austenitic phase in the laser-melted samples of Li et al. was high enough to induce the formation of martensite instead of ferrite [17,18]. The lattice parameter measurements of particles in the as-atomized state from ND and HEXRD are also shown in Figure 5. As these values are almost identical and consistent with the value calculated from the XRD results, the use of the Rietveld analysis to determine lattice parameters from XRD data is validated.

By performing a similar analysis for particles produced via IA in He, and also WA, one can plot the percent of transformation at 550°C as a function of particle undercooling. As shown in Figure 6, it can be concluded that the particles produced via RS with larger eutectic undercooling have a lower percent transformation during isochronal annealing at 550°C. As an example, for the case of the 600-710µm particles produced via IA in N_2, 90% of the retained austenite has transformed to ferrite, whereas for the 300-355µm particles produced via IA in He, the percent transformed is less than 80%. The percent transformation of particles produced via WA was very low after annealing at 550°C, only about 12% for the 300-355µm particles and 10% for the 90-106µm particles. Thus, larger eutectic undercoolings promote higher tempering stability during annealing since, as shown in Table 1, the eutectic undercooling for WA achieved during RS was approximately 68°C to 84°C, which is larger than that of IA powder particles. Rayment et al. [19] and Peng et al. [20] showed that a delay in carbide precipitation can occur in supersaturated austenite due to the stabilizing effect of alloying elements. Kishitake et al. [21] also reported that the temperature of transformation of retained austenite in rapidly solidified tool steels increases with increasing Cr and Mo content. They showed that the decomposition of the retained austenite

phase could be delayed by the addition of carbide formers, while there is only minor effect by carbon content. Furthermore, although a detailed mechanism for this tempering stability is unknown, it can be hypothesized that the misfit lattice strain caused by the supersaturated alloying elements might be impeding substitutional diffusion of the M elements [16,22]. Finally, the supersaturated alloying elements in the austenite could change the size of interstitial sites and increase the activation energy for carbon diffusion [16,23]. Together, these mechanisms would inhibit the transformation of austenite to ferrite and thus create a lag in carbide precipitation.

Carbide Distribution

The carbide precipitate diameter after annealing was characterized using image analysis. Figure 7 shows the diameter of rod precipitates as a function of RS undercooling for particles produced via IA and WA and then annealed at 650˚C, 750˚C and 810˚C. As can be seen in Figure 7, precipitate diameter increases with annealing temperature, as expected. The effect of RS undercooling on precipitate diameter is less apparent. For annealing at 650˚C, the undercooling effect is negligible. At 750˚C and 810˚C, there may be some effect of undercooling on the precipitate diameter, however, the scatter in the data is quite high. For the IA atomized particles, the trend shows a general increase in the precipitate diameter with increasing eutectic undercooling. However, the results from the WA atomized particles do not seem to follow this trend. It is hypothesized that the increase in precipitate diameter with increasing eutectic undercooling, if present, is related to the supersaturation of alloying elements within austenite. It has been reported [25] that chromium diffuses more rapidly in ferrite as compared to most other metallic alloys, with the result being that the Cr_7C_3 carbide is present in microstructure during tempering. Furthermore, chromium carbide coarsens more rapidly as compared to other carbides such as vanadium carbides. Therefore, austenite supersaturated with chromium may cause the precipitates to coarsen more quickly in the powder particles formed at high RS cooling rates thus having larger eutectic undercooling.

Carbide Shape

The mechanical properties of the annealed particles are more fully discussed in the next section; however this data can also be used to infer the shape of the carbides in D2 tool steel. Figure 8 shows the variation in powder particle hardness as a function of precipitate spacing for different annealing temperatures. As expected, the hardness decreases with increasing precipitate spacing,

corresponding to an increase in annealing temperature. It is well known that the variation in powder particle hardness with precipitate spacing can be given by [24]:

$$H = H_0 + A_p r_p^{-d} \qquad\qquad \text{Eq. 3}$$

where H_0 is the initial hardness value, A_p is the known area at which measurements have been done in μm^2, r_p is spacing between precipitates in μm and d is a constant depending on the precipitate shape. Based on the calculated hardness trendline, the value of d for the carbide precipitates in D2 tool steel is 0.38. For aluminum-silicon alloys, the value of d for angular, flaky, and fibrous silicon precipitates has been calculated as 0.5, 0.22, and 0.1, respectively [24]. Thus, it can be hypothesized that the rod-shaped carbides in the D2 tool steel are intermediate in geometry between angular and flaky shapes.

Mechanical Properties of the D2 Tool Steel RS Powder Particles

The effect of the isochronal annealing on the microhardness of D2 tool steel is shown in Figure 9.a. The results for the particles with the highest and lowest undercooling during IA, 300-355μm (He) and 600-710μm (N$_2$), respectively, are shown, along with the WA-produced particles in the 300-355μm size. The hardness for each particle family in the as-atomized condition is also given for comparison purposes (open symbols at an annealing temperature of 25˚C). As can be seen, the particles in the as-atomized state produced via IA show almost a similar hardness values. Annealing of the particles at 350˚C and 450˚C revealed almost no significant change in the hardness as compared to the as-atomized state. As shown in Figure 5, precipitation is not occurring at these annealing temperatures. At the 550˚C annealing temperature, the hardness increases substantially. This temperature produced the peak hardness for the IA-produced particles (although further study would be needed to refine the peak temperature), while the peak occurs in the WA particles at approximately 650˚C. Above these peak temperatures, the hardness drops substantially. It should be noted that for WA particles, although the trend shows an increase in the hardness at the annealing temperature of 550°C, according to the size of the error bars, the data is inconclusive.

The difference in peak hardness between the two sets of particles produced via IA can be linked to the difference in percent transformed at 550˚C, shown in Figure 6. The larger percentage of austenite to ferrite transformation in the 600-710μm particles produced via IA in N$_2$ (90 percent)

9

compared to that in the 300-355µm particles produced via IA in He (80 percent) enabled additional carbides precipitation, resulting in strength enhancement. The difference in peak annealing temperatures between the IA and WA can also be linked to the percent transformed, since only about 12 percent of phase transformation occurred for the 300-355µm WA powder particles at an annealing temperature of 550˚C. The loss in hardness above the peak values at 750°C and 810°C annealing temperatures is because of the coarsening of precipitates and grain growth.

Figure 9.b shows the variation in hardness as a function of annealing temperature of the D2 steel after laser surface melting (LSM) [26], conventional quenching from an austenitization temperature of 1025°C [2], and RS-produced particles produced in this study (600-710µm in size; produced via IA in N_2). As can be seen, the peak hardness is obtained for LSM at a temperature of 600°C and a maximum hardness of 620HV0.1, for conventional hardening at 500°C and 570HV0.1, and for the RS particles at 550°C and 650HV0.1. Thus, the RS-produced particles had the highest hardness. On the other hand, the hardness of IA and LSM samples annealed at lower temperatures are much lower as compared to the conventionally treated sample. Retained austenite in IA and LSM differs from the retained austenite after conventional quenching, because while the latter decomposes during tempering in the 200-350°C temperature range [26], the present work and [26] show that IA and LSM – produced retained austenite only transforms after tempering at 550°C and 600°C, respectively. As mentioned previously, retained austenite present after rapid solidification is largely supersaturated with alloying elements whereas in conventional quenching the system is closer to equilibrium, with the alloying elements present as carbides. It is noted that segregation of interstitial solute atoms to austenite dislocation should contribute to stabilizing the retained austenite [26]. It also seems that, for these materials, the destabilization of austenite occurs after the M_7C_3 phase undergoes precipitation. Thus, during the formation of the precipitates, the retained austenite phase becomes depleted from alloying elements, allowing the austenite to ferrite transformation to occur. These factors may be responsible for the observed shift in the secondary hardening peak from 500°C to 550°C in IA and to 600°C in LSM.

Conclusions

Rapid solidification through impulse atomization (IA) and water atomization (WA) has been applied to D2 tool steel, followed by isochronal annealing at different temperatures between 350˚C and 810˚C. Rietveld analysis of the as-atomized powders shows that during rapid

solidification of this alloy, supersaturation of alloying elements results in the formation of retained austenite with a 0.3615 nm lattice parameter. Particles with larger eutectic undercooling have larger amounts of supersaturation of austenite with alloying elements. XRD analysis of the annealed powders shows that primary retained austenite supersaturated in alloying elements transforms to ferrite and carbide precipitates during annealing. A maximum hardness of 620HV was achieved during annealing at 550°C. This is a higher hardness value than for conventional processing of D2 tool steel, which is due to the precipitation of fine and well-distributed carbides during annealing.

Based on the current study, it appears that there is a strong link between the solidification conditions during RS, and phase transformation during annealing. It has been shown that larger undercooling (and cooling rate) during RS delays the onset of the transformation of austenite to ferrite + carbide during annealing. Thus, an increase in the annealing temperature is required to achieve peak hardness. Once the transformation starts, some evidence for coarsening occurring more rapidly was observed in the samples with larger undercooling. It was hypothesized that this may be due to a larger driving force for carbide growth.

Acknowledgments

References

[1] S. Wang, L. Song, Y. Qiao, M. Wang, Effect of Carbide Orientation on Impact-Abrasive Wear Resistance of High-Cr Iron Used in Shot Blast Machine, Tribol. Lett. 50 (2013) 439–448.

[2] G. Roberts, G. Krauss, R. Kennedy, Tool Steels, 5th ed., ASM International, Ohio, 1998.

[3] Y. Dai, M. Yang, C. Song, Q. Han, Q. Zhai, Solidification structure of C2.08Cr25.43Si1.19Mn0.43Fe70.87 powders fabricated by high pressure gas atomization, Mater. Charact. 61 (2010) 116–122.

[4] A.K. Bhargava, A.N. Tiwari, Some Microstructure Aspects of Melt-Spun D2 Steel, Trans. Indian Inst. Met. 58 (2005) 41–47.

[5]   A.K. Bhargava, A.N. Tiwari, Effect of rapid solidification and heat treatment on D2 steel, Int. J. Rapid Solidif. 7 (1992) 51–66.

[6]   P. Delshad Khatibi, H. Henein, A. Ilbagi, Microstructural Investigation of D2 Tool Steel during Rapid Solidification Using Impulse Atomization, in: TMS 2011 Conf., San Diego, California, 2011.

[7]   P. Delshad Khatibi, D.G. Ivey, H. Henein, Effect of rapid solidifiation and heat treatment on D2 tool steel, in: TMS 2012 Conf., Orlando, FL, United States, 2012.

[8]   C. Leguen, Prior austenite grain size controlled by precipitates, The National Institute of Applied Sciences of Lyon, 2010.

[9]   Andersson J.O., Helander T., Höglund L., Shi P.F., and Sundman B. (2002) Thermo-Calc and DICTRA, Computational tools for materials science. Calphad, 26, 273-312.

[10]   P. Delshad Khatibi, A. B. Phillion, H. Henein, Microstructural investigation of D2 tool steel during rapid solidification, Powder Metall. 57 (2014) 70-78.

[11]   H. Henein, Single fluid atomization through the application of impulses to a melt, Mater. Sci. Eng. A. 326 (2002) 92–100.

[12]   M. Covaciu, T. Canta, E. Gordo, Characterization and Sinterability Study of P.M. High-Speed Steel Obtained by Water Atomization, Adv. Mater. Res. 23 (2007) 147–150.

[13]   Y. Seki, S. Okamoto, H. Takigawa, N. Kawai, Effect of atomization variables on powder characteristics in the high-pressured water atomization process, Met. Powder Rep. 45 (1990) 38–40.

[14]   Schneider, C.A., Rasband, W.S., Eliceiri, K.W. "NIH Image to ImageJ: 25 years of image analysis". Nature Methods 9, 671-675, 2012.

[15]   P. Delshad Khatibi, Microstructural investigation of D2 tool steel during rapid solidification, PhD thesis, University of Alberta (2014)

[16]   M.Y. Li, Y. Wang, B. Han, The Kinetics of Phase Transformations During Tempering in Laser Melted High Chromium Cast Steel, J. Mater. Eng. Perform. 21 (2011) 1091–1098.

[17]   A.M. Bayer, T. Vasco, L.R. Walton, Wrought Tool Steels, Properties and Selection: Irons, Steels, and High-Performance Alloys, in: ASM Handb., ASM International, 1990: pp. 757–779.

[18]   A. Lesko, E. Navara, Microstructural Characterization High-Carbon Ferrochromium, Mater. Charact. 36 (1996) 349–356.

[19]   J.J. Rayment, B. Cantor, The As-Quenched Microstructure and Tempering Behavior of Rapidly Solidified Tungsten Steels, Metall. Trans. A. 12 (1981).

[20]   Q.F. Peng, Z.F. Shi, I.M. Hancock, a. Bloyce, Energy Beam Surface Treatment of Tool Steels and their Wear, Key Eng. Mater. 46-47 (1990) 229–244.

[21]   K. Kishitake, H. Era, F. Otsubo, Structures and Tempering Behavior of Rapidly Solidified High-Carbon Iron Alloys, Metall. Trans. A. 22 (1991) 775–782.

[22]   G. Zając, J. Pacyna, The kinetics of phase transformations during tempering in structural steels with nickel, J. Mater. Process. Technol. 162-163 (2005) 442–446.

[23]   J. Wang, R.L. Zuo, Z.P. Sun, C. Li, H.H. Liu, H.S. Yang, et al., Influence of secondary carbides precipitation and transformation on hardening behavior of a 15 Cr–1 Mo–1.5 V white iron, Mater. Charact. 55 (2005) 234–240.

[24]   Khan, A. Ourdjini, Q.S. Hamed, M.A. AlamNajafabadi, R. Elliot, Hardness and mechanical property relationships in directionally solidified aluminium-silicon eutectic alloys with different silicon morphologies, J. Mater. Sci. 28 (1993) 5957–5962.

[25]   M. Maalekian, The Effects of Alloying Elements on Steels, 2007.

[26] R. Colaco, R. Vilar, Effect of laser surface melting on the tempering behaviour of DINX42Cr13 stainless tool steel, Scr. Mater. 38 (1997) 107–113.

[27] K. Zumsande, N. Krasokha, S. Huth, S. Weber, W. Theisen, In situ investigation of the gas-solid interaction between high-alloyed steel powder and nitrogen by energy dispersive diffraction, J. Mater Sci. 47 (2012) 3214-3226.

Table Captions:

Table 1. Experimental data from [10] linking eutectic fraction, cooling rate, and eutectic undercooling during RS

Atomization technique	Atomization atmosphere	Cooling Rate (˚C/s)	Eutectic Undercooling (˚C)	Eutectic Fraction (-)
IA	He	7,622	68	11
		1,589	64	11.4
		538	54	14
IA	N_2	1,778	62	12.5
		434	58	13.5
		212	30	19
WA	N/A	111,945	84	8.3
		16,841	72	10.5
		1,416	68	11.4

Table 2. IA run conditions and atomized particle size distribution

Atomization technique	Atomization atmosphere	Number of orifices	Orifice size (μm)	D50 (μm)	σ
IA	He	37	420	670	1.16
	N_2	37	400	510	1.22

$$\sigma = \frac{D84}{D50}$$

Figure Captions:

Figure 1. XRD patterns for IA 600-710 µm powder particles atomized in nitrogen and then annealed for 2 hours at different temperatures between 350°C and 810°C. Note that for the as-atomized particle, the cooling rate during RS was 434°C/s.
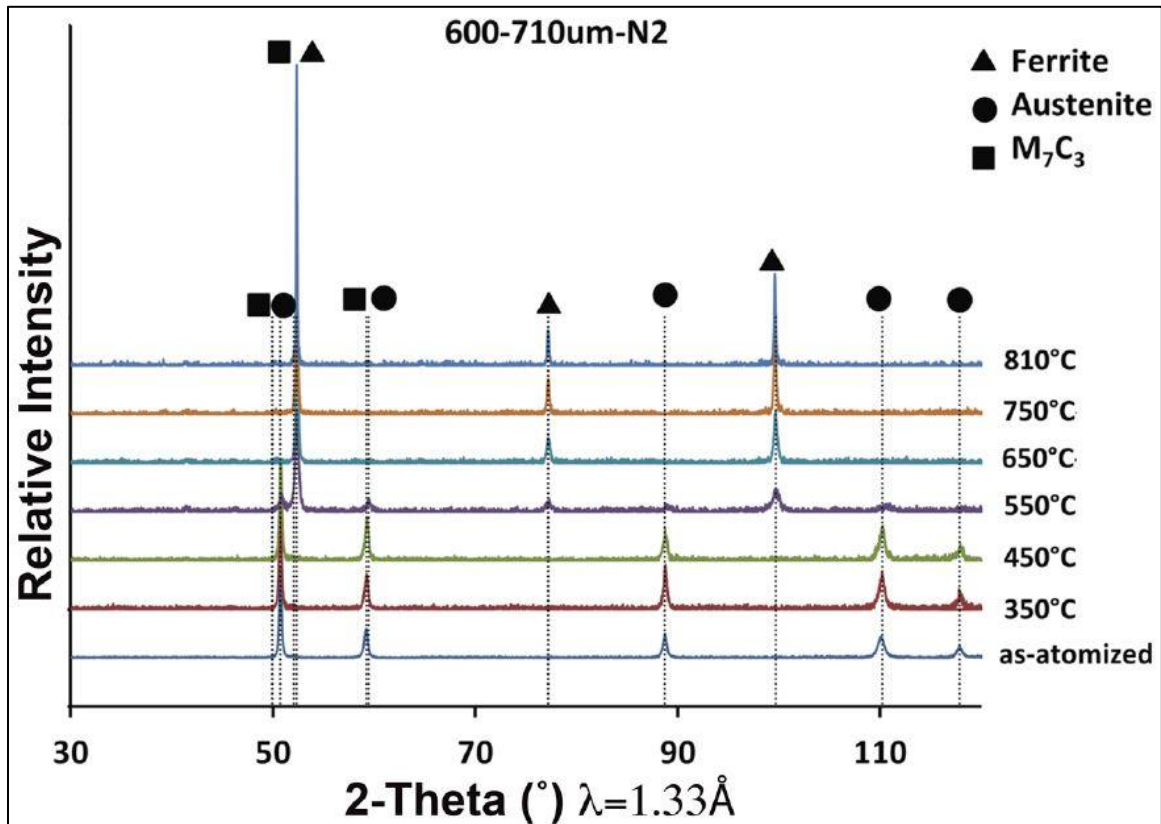
Figure 2. SEM images of IA particles 600-710µm in size, atomized in nitrogen and then annealed for 2 hours a different temperatures: (a) 550°C, (b) 650°C, (c) 750°C and (d) 810°C. The original as-solidified microstructure (e).

a)

b)

c)

d)

e)
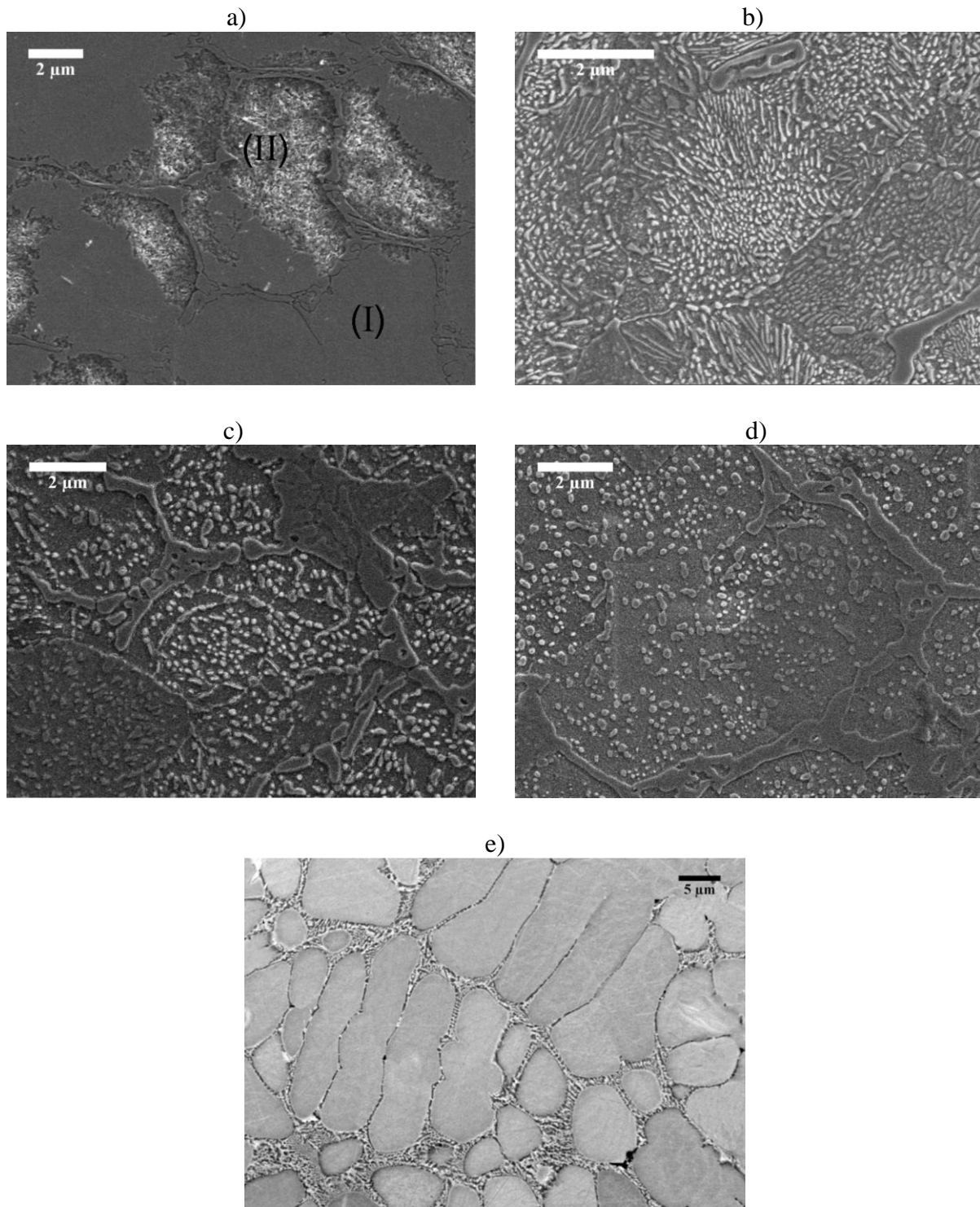
Figure 3. Amount of supersaturation in atomized D2 tool steel after annealing at 550˚C, 650˚C and 750˚C as a function of eutectic undercooling during RS.
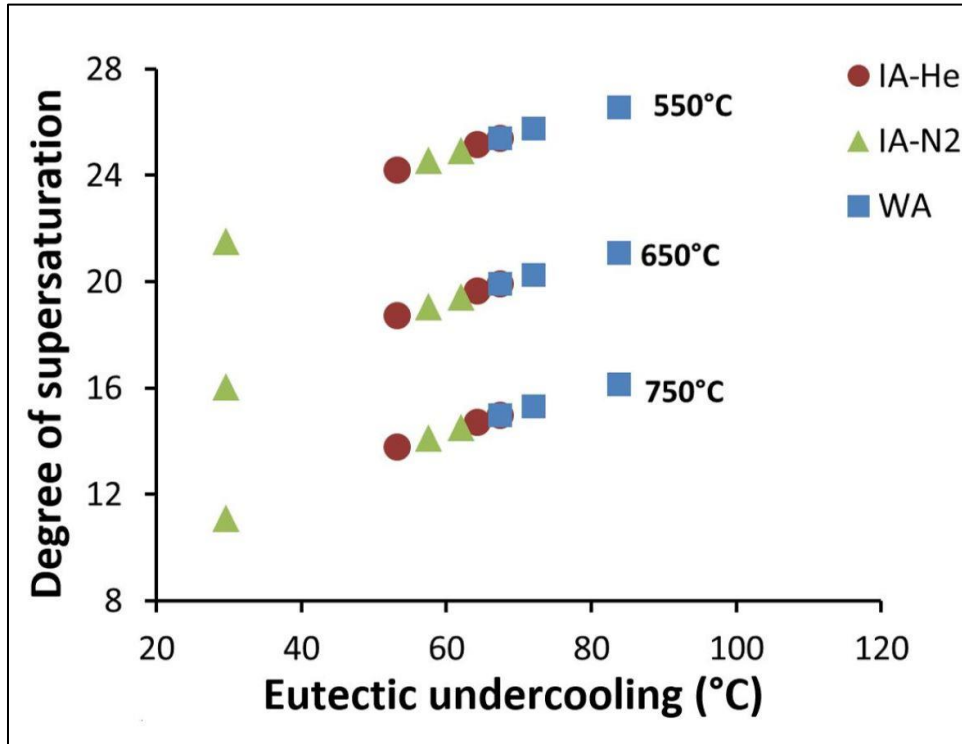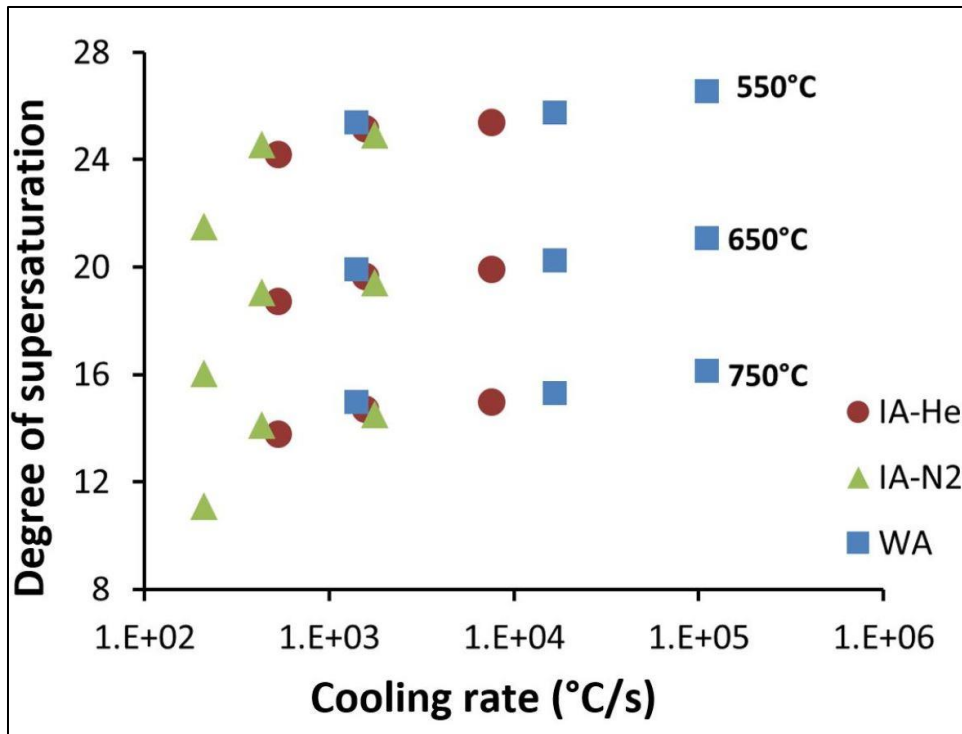

Figure 4. Amount of supersaturation in atomized D2 tool steel after annealing at 550˚C, 650˚C and 750˚C as a function of cooling rate during RS.

Figure 5. Lattice parameter of austenite and percent transformation of austenite to ferrite as a function of annealing temperature for IA powder particles atomized in nitrogen.
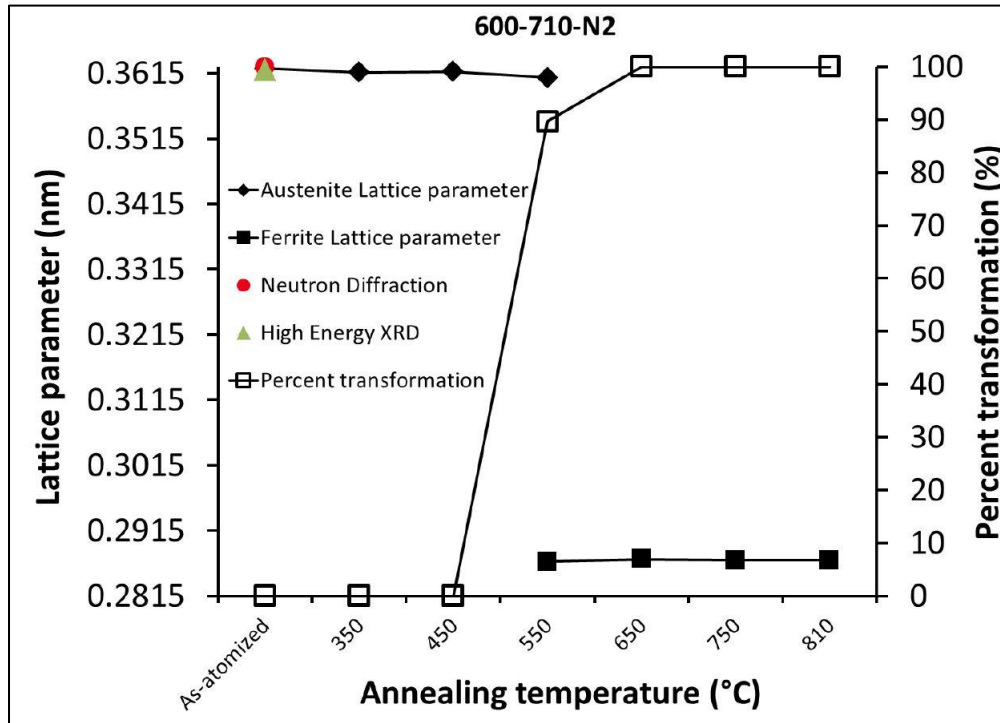
Figure 6. Percent of transformation of austenite to ferrite at 550°C as a function of eutectic undercooling during RS.
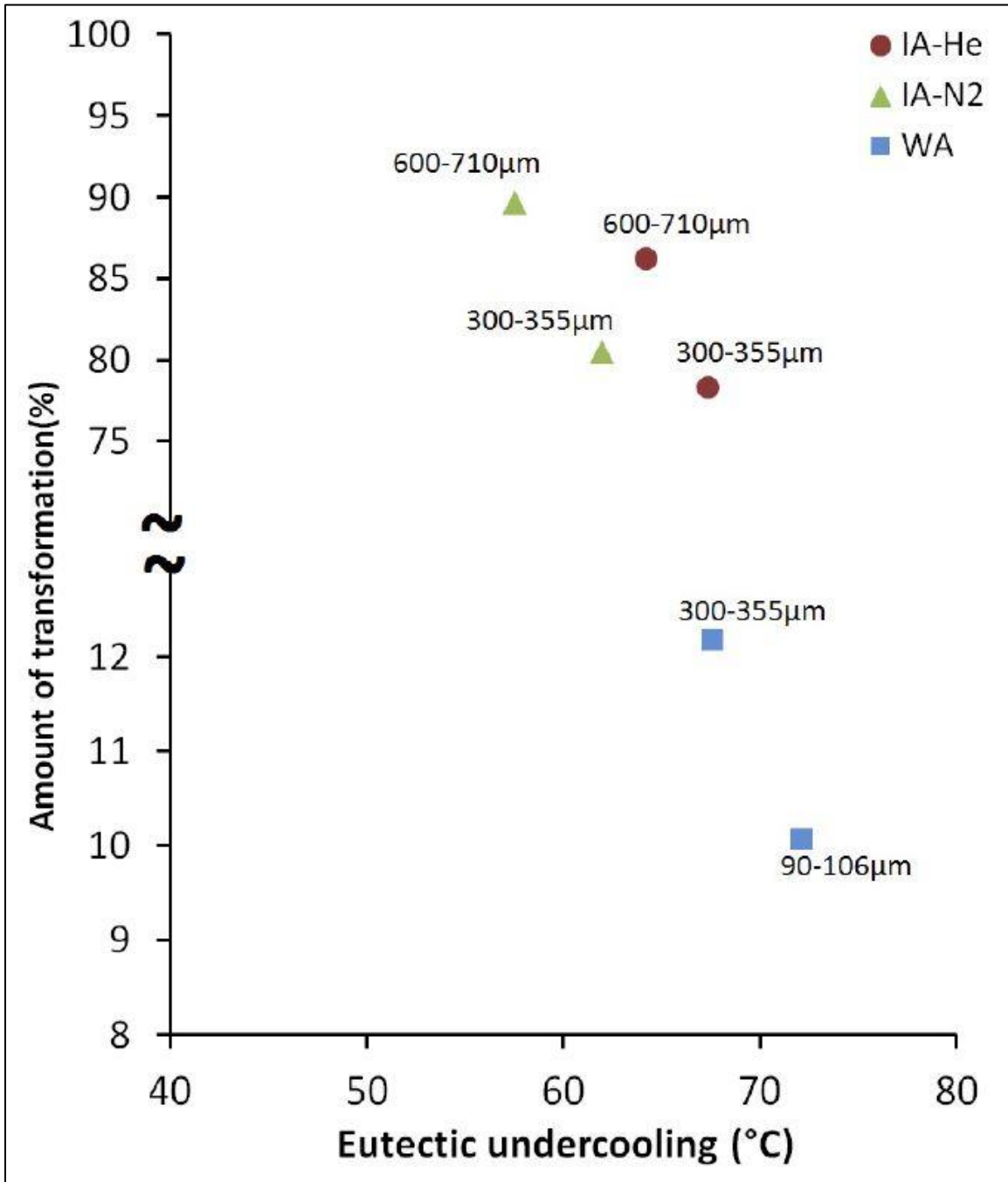
Figure 7. Precipitate diameter in atomized D2 tool steel after annealing at 550˚C, 650˚C and 750˚C as a function of eutectic undercooling during RS.
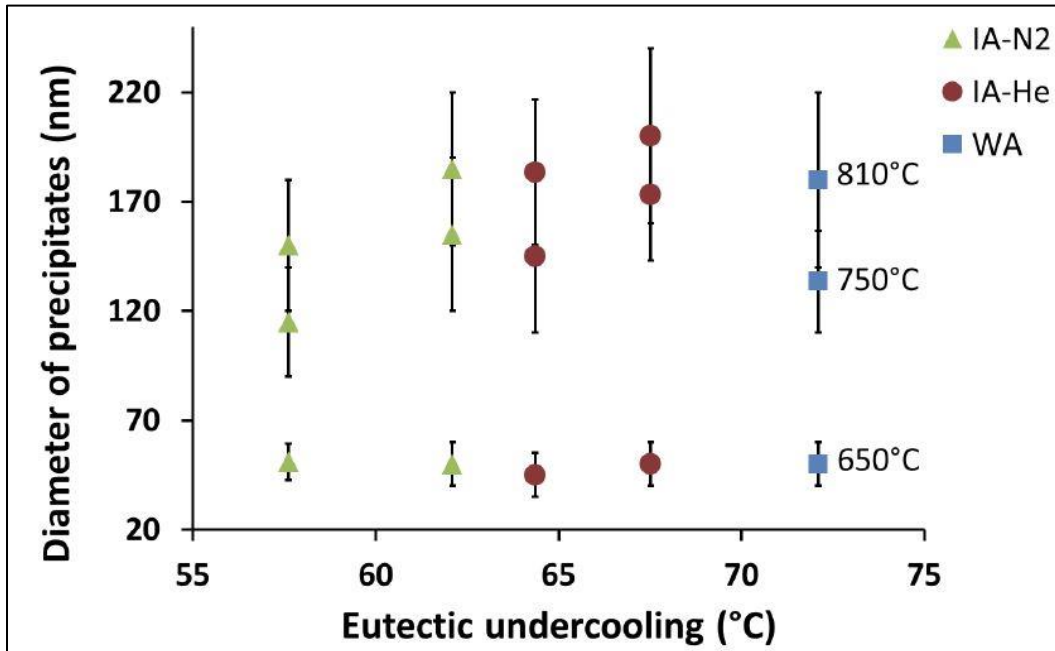

Figure 8. Powder particle Vickers hardness (HV0.1 scale) as a function of precipitate spacing for powder particles annealed at different temperatures.
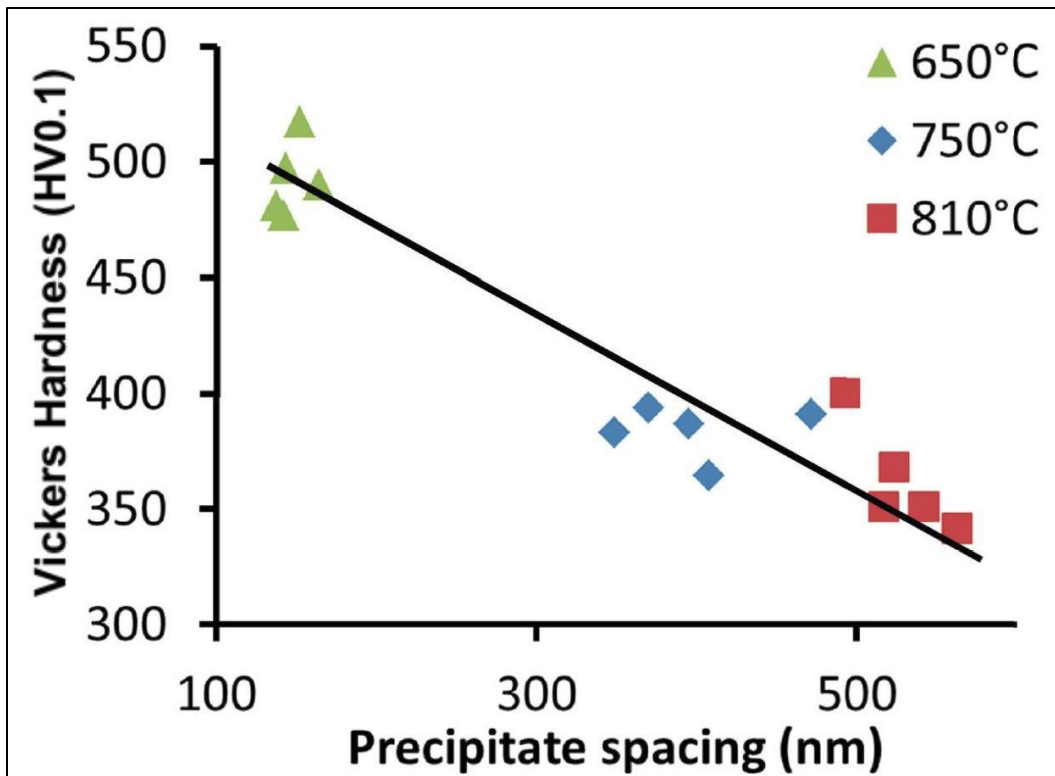
Figure 9. Vickers hardness comparison at the HV0.1 scale, (a) as-atomized D2 tool steel droplets of different sizes and atomized in different atmospheres, as well as annealed samples at different temperatures; (b) laser melted and conventionally treated D2 tool steel along with IA solidified particles.

a)

b)